Research Square

Preprints are preliminary reports that have not undergone peer review.
They should not be considered conclusive, used to inform clinical practice,
or referenced by the media as validated information.

A Hybrid Source for Deterministic Generation of Atom-Photon Entangled States

Priyanshu Tiwari

priyanshu.tiwari@uni-paderborn.de

Paderborn University

Aleksa Krstic

Friedrich Schiller University Jena

Frank Setzpfandt

Friedrich Schiller University Jena

Robert Loew

University of Stuttgart

Sina Saravi

Paderborn University

Article

Keywords: quantum optics, quantum networks, atom--photon entanglement, cavity QED

Posted Date: July 16th, 2026

DOI: https://doi.org/10.21203/rs.3.rs-10319323/v1

License: This work is licensed under a Creative Commons Attribution 4.0 International License.
Read Full License

Additional Declarations: No competing interests reported.

A Hybrid Source for Deterministic Generation of Atom-Photon Entangled States

Priyanshu Tiwari[1,2,3*], Aleksa Krstić[3], Frank Setzpfandt[3,4], Robert Löw[5], Sina Saravi[1,2,6,3]

[1] Heinz Nixdorf Institute, Paderborn University, Fürstenallee 11, 33102, Paderborn, Germany .

[2] Department of Electrical Engineering and Information Technology, Paderborn University, Warburger Straße 100, 33098, Paderborn, Germany .

[3] Institute of Applied Physics, Abbe Center of Photonics, Friedrich Schiller University Jena, Albert-Einstein-Straße 15, 07745, Jena, Germany .

[4] Fraunhofer Institute for Applied Optics and Precision Engineering, Albert-Einstein-Straße 7, 07745, Jena, Germany .

[5] Physikalisches Institut, Universität Stuttgart, Pfaffenwaldring 57, 70569, Stuttgart, Germany .

[6] Institute for Photonic Quantum Systems (PhoQS), Paderborn University, Warburger Straße 100, 33098, Paderborn, Germany .

*Corresponding author(s). E-mail(s): priyanshu.tiwari@uni-paderborn.de;

Abstract

In this work, we propose a scheme for the generation of atom–photon entangled states in a hybrid system comprising a $\chi^{(2)}$ nonlinear medium and a multilevel atom, both embedded inside a cavity. Under appropriate tuning of the pump, cavity modes, and control-pulse frequencies, a pump photon is coherently down-converted into a single cavity photon while simultaneously exciting the atom, thereby generating a joint atom–photon excitation. In this setting, it is possible to generate an entangled state between the photon and the atom. By generating the excitation directly within the atomic system, importantly, this approach avoids the fundamental inefficiencies that arise when interfacing single photons with quantum memories. The nonlinear medium is driven by a pump pulse,

while a control pulse transfers the atomic excitation to long-lived memory states. The properties of the emitted photon, particularly its central frequency, are determined by the interplay between the pump, control field, and cavity modes, providing the flexibility to tailor the emitted photon to existing quantum communication channels. Thus, the proposed scheme offers a promising route toward the realization of quantum repeater nodes in quantum networks.

Keywords: quantum optics, quantum networks, atom–photon entanglement, cavity QED

Introduction

Quantum networks [1–4] comprise coherent communication channels that preserve quantum information during transmission, and quantum nodes that generate, process, and store it. Optical photons are particularly well suited as carriers of quantum information due to their low propagation losses, compatibility with existing telecommunication networks, and robust qubit encodings such as polarization [5–7]. Realization of quantum nodes, therefore, requires an efficient interface for coherent exchange of quantum information between stationary qubits and propagating photonic modes [7]. In this context, stationary qubits function as quantum memories (QMs), ensuring high-fidelity storage and retrieval of quantum states. In such photonic networks, one of the most widely implemented approaches to quantum nodes relies on absorptive quantum memories (QMs) [8–10]. In this scheme, a photon-pair source and a stationary qubit (acting as a QM) are placed at each node. One photon from an emitted pair is stored locally in the qubit while the other is transmitted. The photons emitted from neighboring nodes are then interfered in a Bell-state measurement, which heralds entanglement between the remote QMs [2, 11–14]. The performance of such node architectures therefore depends crucially on an efficient interface between stationary QMs and propagating photonic modes, making this interface a central requirement for large-scale quantum networks. QMs can be realized in a range of systems with long coherence times, including trapped atoms or ions, atomic vapours, rare-earth-ion-doped crystals, and solid-state spin systems [15–20]. Photon-pair sources, on the other hand, are commonly based on nonlinear processes such as parametric down-conversion (PDC) [21, 22] and spontaneous four-wave mixing (SFWM) [23, 24]. These sources offer broad control over the spectral, spatial, and polarization properties of the generated states [25], and in nondegenerate schemes one photon can be tailored for transmission while the other is mapped to a particular quantum memory [25–27]. However, due to the inherent probabilistic nature of photon-pair generation via PDC and SFWM [28], together with imperfect photon–memory interfacing efficiencies arising from residual mode mismatch [29, 30], the overall probability of generating a photon entangled with the internal states of a QM is substantially reduced. Such a probabilistic operation constitutes a major hurdle in the development of scalable quantum networks.

Another promising route uses single quantum emitters in free space [31], which can deterministically emit a single photon entangled with the internal state of the emitter [32]. In free space, however, the light–matter interaction is typically too weak to enable efficient and reversible exchange of quantum information between a photonic channel and a single emitter, as the atomic absorption cross section is much smaller than the cross-sectional area of the incident optical beam [33]. Cavity-QED-based schemes address this limitation by strongly coupling an atom to a cavity mode, enabling deterministic atom–photon entanglement generation, for example via vSTIRAP [33–37]. However, these schemes usually produce photons in the visible or near-infrared ranges, and the emission frequency is largely fixed by the atomic transition, which limits spectral tunability and compatibility with telecommunication wavelengths. One possible solution is to employ quantum frequency conversion to convert the frequency of single photons from visible or near infrared into the telecom range suitable for long-distance communication [38, 39]. However, this approach is limited by conversion efficiency, leading to a reduction in the probability of generating an atom–photon entangled state.

In this paper, we propose a hybrid system for quantum nodes that combines a nonlinear PDC source with a multilevel atom inside an optical cavity and enables the deterministic generation of frequency-tunable atom–photon entangled states, as depicted in Fig. 1(a). Our approach builds on the concept of atom-mediated spontaneous PDC introduced in Ref. [40]. In that proposal, the nonlinear photonic environment is engineered to suppress down-conversion by eliminating the relevant final states for one of the generated photons. A resonant two-level emitter then provides a discrete alternative degree of freedom that can host the missing excitation, while its fermionic two-level structure suppresses higher-order pair generation. Here, we extend this idea beyond the spontaneous regime to enable on-demand generation of atom–photon entanglement, where the polarization of a generated single photon is entangled with the internal states of an atom.

In our scheme, we consider a multilevel atom coupled to the modes of an optical cavity containing a nonlinear $\chi^{(2)}$ medium. Related hybrid architectures combining nonlinear processes with quantum emitters have recently attracted interest for quantum state engineering and entanglement generation [41–44]. In our configuration, the cavity resonances are deliberately detuned from the frequencies required for efficient PDC. As a result, the PDC process is suppressed within the cavity, while the atom provides the additional degree of freedom necessary to facilitate the down-conversion process. In this way, pump driving generates a cavity photon together with an atomic excitation, yielding an entangled state between the polarization of the emitted photon and the internal excited states of the atom. By operating in the high-gain regime and shaping the pump pulse appropriately, this atom–photon entangled state can be generated on demand. We then introduce a control pulse that drives the excited states to long-lived atomic states, thereby preserving the entanglement by storing it in a long-lived atomic memory. Since the spectral modes and output spatial modes of nonlinear optical cavities can be strongly tailored, such a system can, in principle, be engineered for efficient coupling to optical fibers or free-space channels without the need for extra postprocessing, such as quantum frequency conversion. Simultaneously, this hybrid

approach overcomes both the problems of the probabilistic nature of photon-pair generation in nonlinear sources and coupling between photon-pair sources and quantum memories, altogether by using the hybrid approach. Hence, the proposed hybrid system provides a promising, versatile building block for quantum node architectures.

The outline of the paper is as follows. In Sec. 1, we introduce the hybrid system and provide a brief overview of the proposed protocol. In Sec. 2, we present a theoretical description of the operating principle of the hybrid system using a step-by-step approach, gradually increasing the level of system complexity. We then analyze the effects of cavity losses and atomic spontaneous emission, and discuss how these processes influence the generation probability of the atom–photon entangled state. Finally, in Sec. 3, we summarize our conclusions.

1 The Hybrid System

In this section, we introduce the proposed hybrid system designed to generate entanglement between the polarization degree of freedom of a single photon and the internal quantum states of an atom. The system comprises of a nonlinear $\chi^{(2)}$ media embedded in a cavity, as depicted in Fig. 1(a). The cavity supports two frequency-degenerate idler modes at frequency ω_i and two degenerate signal modes at frequency ω_s. For each frequency manifold, the two modes are mutually orthogonal, corresponding to right-circular (R) and left-circular (L) polarizations, as shown in Fig. 1(b). For reference, the nonlinear cavity is engineered such that, in the absence of the atomic system, it generates a frequency-nondegenerate, polarization-entangled photon-pair state of the form $\frac{1}{\sqrt{2}}\left(|1_{L_i}, 1_{R_s}\rangle + |1_{R_i}, 1_{L_s}\rangle\right)$ when operated in the SPDC (low-gain) regime and pumped with a pump beam of frequency $\omega_p = \omega_s + \omega_i$. However, in the present work, the cavity resonances are intentionally detuned from this condition. Here, the idler photon, with circular polarization states $|1_{L_i}\rangle$ or $|1_{R_i}\rangle$, is maximally entangled in the polarization degree of freedom with the signal photon, with states $|1_{L_s}\rangle$ or $|1_{R_s}\rangle$.

The hybrid system then consists of this nonlinear cavity, along with a multilevel atom serving as a quantum memory embedded in it. The relevant energy levels of the atom are shown in Fig. 1(c), and comprise a ground state $|g\rangle$, two degenerate excited states $|e_1\rangle$ and $|e_2\rangle$ with transition energies $\hbar\omega_e$ (with respect to $|g\rangle$), and two degenerate long-lived states $|m_1\rangle$ and $|m_2\rangle$ separated from the ground state by an energy $\hbar\omega_m$. The employed level structure is representative of a class of atomic (or atom-like) systems commonly used for quantum memories, such as alkali atoms (e.g., rubidium or cesium) [45, 46]. For concreteness, we consider an atomic-level scheme inspired by the ^{87}Rb quantum memory demonstrated in Ref. [47]. An explicit mapping to the corresponding ^{87}Rb hyperfine states is provided in the Supplementary Material(see Sec. S5). The idler modes of the cavity couple to the atomic dipole transitions connecting the ground state $|g\rangle$ to the excited states $|e_j\rangle$ ($j = 1, 2$). Here we assumed that the L polarized idler mode drives the transition $|g\rangle \leftrightarrow |e_1\rangle$ and R polarized idler mode drives the transition $|g\rangle \leftrightarrow |e_2\rangle$, consistent with angular-momentum selection rules. Finally, to transfer the excitation from the atomic excited states to the long-lived states, we drive the atom with a control pulse as shown in Fig. 1(a). The control pulse has a π polarization, enabling the atomic transition from $|e_i\rangle \rightarrow |m_i\rangle$ [47, 48].

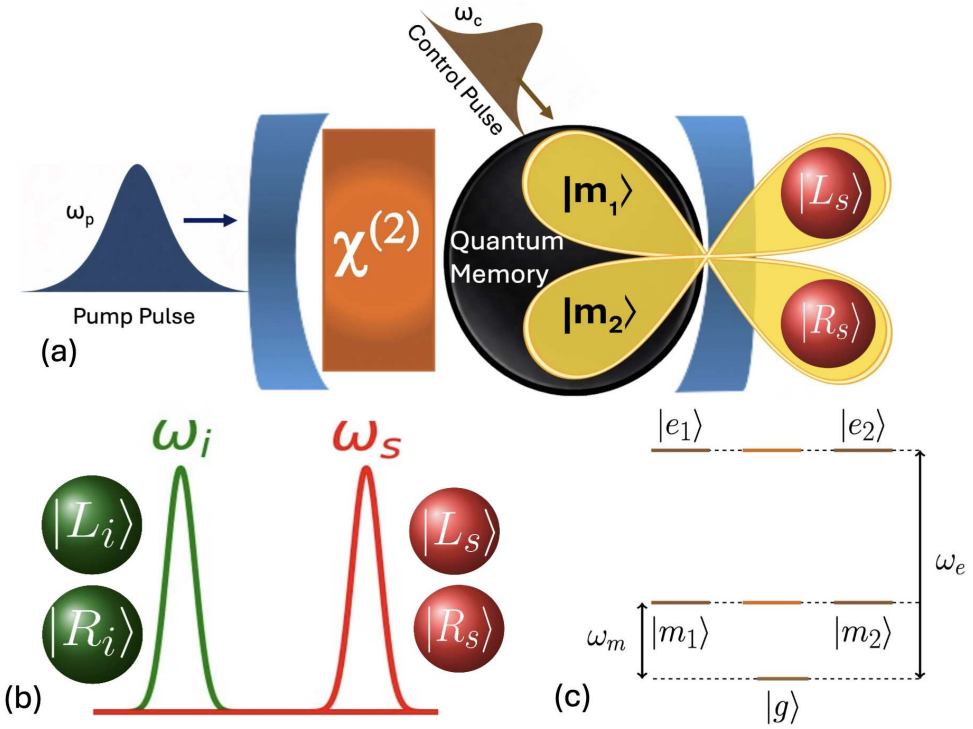


Fig. 1: **(a)** Schematic of the proposed setup. A pump pulse at frequency ω_p, detuned from the conventional PDC resonance condition $\omega_p = \omega_s + \omega_i$, drives a $\chi^{(2)}$ nonlinear cavity. The cavity modes are coupled to an atomic quantum memory through the idler modes, while a control pulse at ω_c couples the excited atomic states to long-lived states. **(b)** Cavity optical modes spectrum highlighting the signal and idler resonances, each supporting two frequency-degenerate modes with orthogonal polarizations, where in our example we choose left- (L) and right-circularly (R) polarized modes. **(c)** Atomic level structure of our quantum memory showing the ground state $|g\rangle$, long-lived states $|m_1\rangle, |m_2\rangle$, and excited states $|e_1\rangle, |e_2\rangle$, along with relevant transition frequencies ω_m and ω_e.

The system allows for two possible configurations for generating atom–photon entangled states. One omits the control pulse and generates a state in which the entanglement is shared between the excited states of the atom $\{|e_i\rangle\}$ and the polarization of the signal photon. Such entangled states can serve as building blocks for the generation of larger multipartite entangled states, including cluster and GHZ states [49, 50]. The second approach involves a control pulse and generates an atom–photon entangled state in which the entanglement is shared between the long-lived atomic states $\{|m_i\rangle\}$ and the polarization of the signal photon. Such states have applications in quantum node architectures, as discussed in the introduction.

To generate the atom–photon entangled state in which entanglement is shared between the excited states of the atom and the polarization of the signal photon, the nonlinear medium is driven by a pump pulse with a carrier frequency ω_p, while the cavity idler modes drive the atom. Two main interactions occur in this scheme: (i) An off-resonant PDC process, where the pump frequency is chosen such that $\omega_p \neq \omega_i + \omega_s$, resulting in a transient population of the polarization-entangled photon-pair state within the cavity modes. (ii) An off-resonant atom–field interaction, where the idler-mode frequency ω_i is detuned from the atomic transition frequency ω_e, causing the $|g\rangle \leftrightarrow |e_i\rangle$ transition to be driven off-resonantly. Although each process is non-resonant, by carefully choosing the detunings, their combined action can result in an overall energy-conserving higher-order process if the energy of a single pump photon equals the combined energy of the signal photon and the atomic excitation, i.e., $\hbar\omega_p = \hbar\omega_s + \hbar\omega_e$. This results in the generation of an entangled atom–photon state of the form $\frac{1}{\sqrt{2}}|1_{R_s}, e_1\rangle - \frac{1}{\sqrt{2}}|1_{L_s}, e_2\rangle$. The off-resonant driving of the PDC process plays a key role in suppressing signal and idler photon buildup in the cavity and restricting their presence to transient excitations. The presence of the atom provides that extra free state that allows the pump photon to efficiently down-convert into a signal photon and an atomic excitation [40]. In this way, the scheme avoids the need to load a previously generated photon into the atom. Since there are no further high-energy states in the atom with $\hbar\omega_e$ energy difference above the excited state, the generation of two or more excitations in the signal mode is suppressed. Thus, with a carefully selected length and amplitude for the pump pulse, our system can ensure the generation of a pure single-photon entangled with the atom.

To generate an atom–photon entangled state in which the entanglement is shared between the long-lived atomic states and the polarization of the signal photon, the atom is additionally interacted with a control pulse of carrier frequency ω_c. In this scheme, three main interactions occur in a higher-order process. The first two interactions are similar to those described previously, although with a different pump frequency, while the third process is given by (iii) the control pulse off-resonantly driving the transition $|e_{1,2}\rangle \leftrightarrow |m_{1,2}\rangle$. The three detunings are chosen such that the following energy conservation condition is satisfied: $\hbar\omega_p = \hbar\omega_s + \hbar\omega_m + \hbar\omega_c$. This condition enables the pump photon to be converted into a signal photon in the cavity while the remaining excitation is shared between the atomic long-lived state and the control field. As a result, the overall resonant interaction generates an atom–photon entangled state in which the entanglement is shared between the long-lived atomic states and the polarization of the signal photon, generating the state $\frac{1}{\sqrt{2}}|1_{R_s}, m_1\rangle - \frac{1}{\sqrt{2}}|1_{L_s}, m_2\rangle$, as depicted in Fig. 1(a).

2 Theoretical Description, Results and Discussion

In this section, we expound on the theoretical description of our system. Since the overall dynamics involves interaction between multiple off-resonant processes, it will be instructive to introduce the underlying physics in steps. To that end, we first discuss on- and off-resonant parametric down-conversion (PDC) processes. We then introduce the multilevel atom inside the cavity and describe the resulting hybrid platform of

atom and nonlinear cavity, emphasizing its functionality as a source of deterministic atom–photon entangled states.

2.1 On- and Off-Resonant Parametric Down Conversion (PDC) in the Nonlinear Cavity

The interaction-picture Hamiltonian governing PDC inside the nonlinear cavity (without the presence of the atom) is

$$\hat{H}_{\mathrm{NL}}(t) = \hbar A_p \mathcal{E}(t) \left[\hat{a}_L^\dagger \hat{b}_R^\dagger + \hat{a}_R^\dagger \hat{b}_L^\dagger\right] e^{-i\Delta_1 t} + \mathrm{H.c.}$$

Here, A_p denotes the effective nonlinear coupling strength, which has units of a rate, and determines how rapidly the system evolves under the PDC process. It is proportional to the peak pump electric field amplitude, the $\chi^{(2)}$ nonlinearity of the medium, and the spatial mode overlap between the pump and the cavity-mode fields [51]. In our numerical simulations, we take A_p to be real and time-independent. We express it in units of Ω, the atom–cavity field coupling strength, which serves as a natural scaling parameter for the system. The envelope $\mathcal{E}(t)$ is dimensionless and describes the slowly varying temporal profile of the pump pulse. The operators $\hat{a}_{L,R}^\dagger$ and $\hat{b}_{L,R}^\dagger$ are the creation operators for the idler and signal modes, respectively. The subscripts L and R denote left-circular and right-circular polarizations, respectively. The detuning $\Delta_1 = \omega_p - \omega_s - \omega_i$ quantifies the mismatch between the pump central frequency ω_p and the sum of the signal and idler frequencies $\omega_s + \omega_i$. When $\Delta_1 = 0$, the process is on resonant, whereas $\Delta_1 \neq 0$ corresponds to an off-resonant PDC process.

We begin by studying the cavity states under both on-resonant ($\Delta_1 = 0$) and off-resonant ($\Delta_1 \neq 0$) driving conditions. To simplify the analysis of the nonlinear process, we first consider continuous-wave (CW) driving, setting $\mathcal{E}(t) = 1$ for all $t \geq 0$. The use of a CW pump allows us to develop physical intuition, as the underlying dynamics are more analytically transparent in this regime. In the pulsed case, the interaction strengths acquire an explicit time dependence through the pulse envelope. However, this does not introduce additional dynamical pathways. Consequently, the qualitative behavior of the system is governed by the same effective processes in both the CW and pulsed regimes. The initial state is taken to be the vacuum state for the cavity modes, denoted as $|0\rangle \equiv |0,0,0,0\rangle$. The four-mode Fock basis is ordered as $|n_{L_i}, n_{R_i}, n_{L_s}, n_{R_s}\rangle$, corresponding respectively to the left- and right-circularly polarized idler and signal cavity modes.

When the nonlinear cavity is driven by a pump field of frequency ω_p on resonance ($\Delta_1 = 0$), it results in the generation of a time-dependent squeezed vacuum state of the form $|\psi_{\mathrm{sq}}(t)\rangle = \frac{1}{\cosh^2(r(t))} \sum_{n=0}^{\infty} \sqrt{n+1}\, \tanh^n(r(t))\, |\phi_n\rangle$, inside the cavity as depicted in Fig. 2a. The parameter $r(t)$ is the interaction strength (squeezing parameter); in the CW case, it is given by $r(t) = A_p t$, and more generally by $r(t) = \int_{-\infty}^{t} A_p \mathcal{E}(t')dt'$ [41]. The squeezing parameter determines the probability of generating the states $|\phi_n\rangle$. Here, $|\phi_n\rangle = \sum_{m=0}^{n} \frac{1}{\sqrt{n+1}} |n-m, m, m, n-m\rangle$, which corresponds to a $2n$-photon polarization-entangled state [28, 52–54]. The $n = 0$ term corresponds to the vacuum

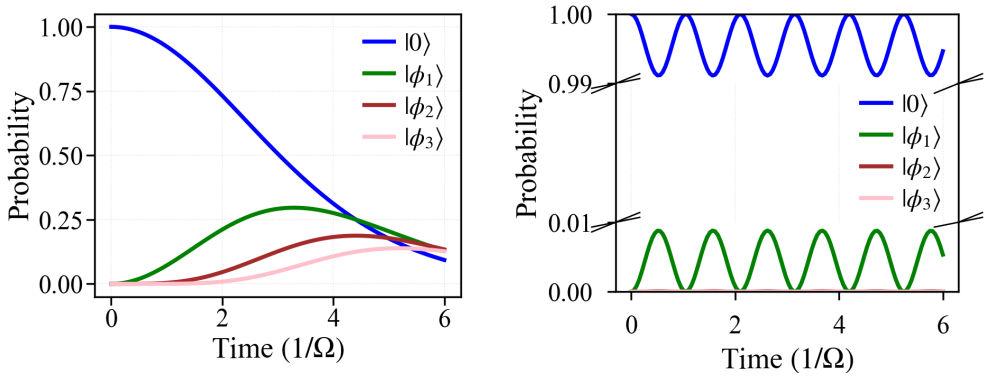


Fig. 2: Investigation of the nonlinear cavity in the absence of the atom. **(a)** On-resonant excitation ($\Delta_1 = \omega_p - \omega_s - \omega_i = 0$) leads to a gradual buildup of the higher-order photon-pair states, or more precisely the $2n$-photon polarization-entangled states $|\phi_n\rangle = \frac{1}{\sqrt{n+1}} \sum_{m=0}^{n} |n-m, m, m, n-m\rangle$. This is accompanied by a depletion of the vacuum state $|0\rangle$ over time. The population of each photon-pair state initially increases, reaches a maximum, and subsequently decreases as population is transferred to higher-order states. **(b)** Off-resonant excitation ($\Delta_1 = 6\Omega$) suppresses the population of the photon-pair states, with $|\phi_2\rangle$ and $|\phi_3\rangle$ remaining negligibly populated, and induces oscillatory dynamics in the states. In both panels, the nonlinear coupling strength is fixed at $A_p = 0.2\Omega$ under continuous-wave (CW) pumping.

state, $n = 1$ to an entangled photon-pair state, and larger values of n describe entangled multi-photon states. The $n = 1$ state, which will play a central role throughout the remainder of this work, has the form $|\phi_1\rangle = \frac{1}{\sqrt{2}} |1_{L_i}, 1_{R_s}\rangle + \frac{1}{\sqrt{2}} |1_{R_i}, 1_{L_s}\rangle$. Here, for brevity, we omit modes with zero photon occupation in our notation, which, when not shown, are implicitly assumed to be in the vacuum state.

Fig. 2a shows the temporal evolution of the occupation probabilities of the lowest four states, $|0\rangle$ through $|\phi_3\rangle$. At the beginning of the interaction, the probability of the vacuum state $|0\rangle$ decreases gradually, while the probability of the state $|\phi_1\rangle$ begins to increase. In this regime, the system operates in the low-gain regime, where the probability of higher-order states $|\phi_{n\geq 2}\rangle$ remains negligible. As the interaction time increases, corresponding to a larger squeezing parameter $r(t)$, the system transitions to the high-gain regime, characterized by a significant population of multi-pair states such as $|\phi_2\rangle$ and $|\phi_3\rangle$. Thus, the probability of generating the state $|\phi_n\rangle$ for $n \geq 1$ initially increases, reaches a maximum, and then gradually decreases. This behavior arises from the coherent redistribution of population among different photon-number states, where higher-order contributions become increasingly significant in the high-gain regime. The maximum probability of generating the state $|\phi_1\rangle$ is approximately 0.30 [28, 53]. This value represents a fundamental limit on the probability of generating an entangled photon pair using PDC, arising from the unavoidable population of higher-order multi-photon states. This limitation is further exaggerated when one of

the photons (e.g., idler) is to be loaded into a Quantum Memory (QM) to generate a light–matter entangled state. Since the coupling to the QM also has a limited efficiency, the overall probability of generating the required atom-photon entangled state will always be smaller than 0.30. Therefore, a nonlinear cavity with its output sent to a QM cannot serve as a deterministic source of atom–photon entangled states.

In the remainder of this work, we show how these intrinsic limitations can be addressed by effectively diverting the idler mode excitations directly into the atom. The central idea is to suppress the generation of the states $|\phi_n\rangle$ for $n \geq 1$, and simultaneously facilitate the buildup of the state $|\psi_{e_1,e_2}\rangle = \frac{1}{\sqrt{2}}|1_{R_s}, e_1\rangle - \frac{1}{\sqrt{2}}|1_{L_s}, e_2\rangle$ or $|\psi_{m_1,m_2}\rangle = \frac{1}{\sqrt{2}}|1_{R_s}, m_1\rangle - \frac{1}{\sqrt{2}}|1_{L_s}, m_2\rangle$ inside the cavity over the interaction period. To suppress the buildup of states $|\phi_n\rangle$ for $n \geq 1$, we use the PDC process in an off-resonant pumping regime ($\Delta_1 \neq 0$). In this regime, the pump frequency is detuned from the condition $\omega_p = \omega_s + \omega_i$, while still assuming perfect phase matching and spatial mode overlap between the pump field and the cavity modes. Under this off-resonant pumping, the population of the $|\phi_n\rangle$ states cannot build up consistently, but rather experiences a repeated constructive and then destructive interference of the generated states. As a result, the net transition amplitude for generating the state $|\phi_n\rangle$ remains small, and the population of the states $|\phi_n\rangle$ exhibits oscillatory behavior. For detunings much larger than the nonlinear coupling strength ($\Delta_1 \gg A_p$), higher-order contributions $|\phi_{n\geq 2}\rangle$ become negligible, while the state $|\phi_1\rangle$ is populated only with a very small probability, as shown in Fig. 2b. In this regime, the dynamics can be accurately described using first-order time-dependent perturbation theory [55]. Within this approximation, the probability of generating the state $|\phi_1\rangle$ is given by $P_{|\phi_1\rangle}(t) = \frac{8A_p^2}{\Delta_1^2}\sin^2\left(\frac{\Delta_1 t}{2}\right)$ (see Supplementary Sec. S1 for a first-order perturbative analysis). As can be seen, the probability is a sinusoidal function with period $2\pi/\Delta_1$, which matches the behavior observed in Fig. 2b.

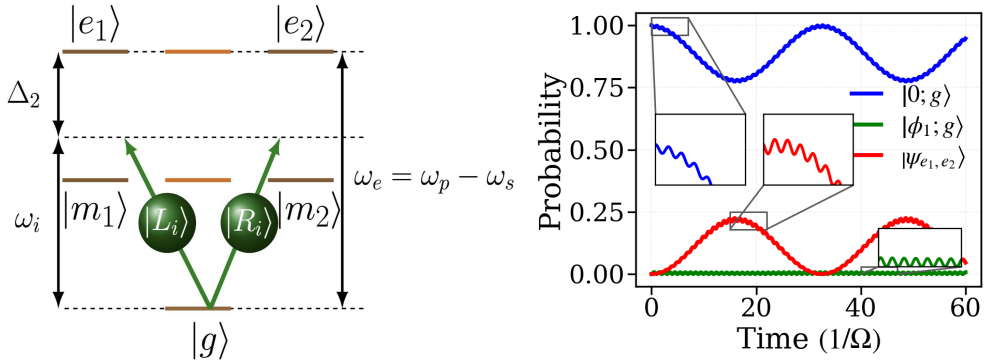
In the following, we show that, in this off-resonant regime, hybridizing the nonlinear source with the atom enables the generated $|\phi_1\rangle$ excitation to be converted into $|\psi_{e_1,e_2}\rangle$ before destructive interference suppresses the cavity excitation. This, in turn, allows atom–photon entangled states to build up.

2.2 Hybrid System of Nonlinear Cavity + Atom

In this section, we study the off-resonant PDC configuration in the presence of a multilevel atom inside the cavity. We consider the atomic transitions $|g\rangle \leftrightarrow |e_{1,2}\rangle$ to be off-resonantly coupled to the idler modes of the cavity with detuning $\Delta_2 = \omega_e - \omega_i$, as depicted in Fig. 3a. Specifically, the left-hand circularly (L_i) polarized idler mode drives the $|g\rangle \leftrightarrow |e_1\rangle$ transition, while the right-hand circularly (R_i) polarized idler mode drives the $|g\rangle \leftrightarrow |e_2\rangle$ transition. The new Hamiltonian of the system is $\hat{H}_{NL}(t) + \hat{H}_{e\leftrightarrow g}(t)$, where the atom-field Hamiltonian under the rotating-wave approximation and in interaction picture [56] is:

$$\hat{H}_{e\leftrightarrow g}(t) = \hbar\Omega\left[\hat{a}_L|e_1\rangle\langle g| - \hat{a}_R|e_2\rangle\langle g|\right]e^{i\Delta_2 t} + H.c.$$

We assume that the orthogonally polarized idler modes have identical spatial mode profiles at the atomic position, and the two atomic transitions $|e_1\rangle \leftrightarrow |g\rangle$ and $|e_2\rangle \leftrightarrow |g\rangle$ have equal and opposite dipole matrix elements, such that the atom-field coupling strength for both transitions have identical magnitude Ω and opposite signs. In the Supplementary Material Sec. 5a, we show that equal coupling strengths for both transitions can be realized using appropriate hyperfine and Zeeman sublevels of ^{87}Rb. The initial state of the atom–field system is $|0; g\rangle \equiv |0\rangle\,|g\rangle$, where all cavity modes are in the vacuum state, and the atom is in its ground state. We will also refer to this as the vacuum state when used in the context of the hybrid system.



(a) (b)

Fig. 3: Investigating the generation of the atom-photon entangled state $|\psi_{e_1,e_2}\rangle = \frac{1}{\sqrt{2}}|1_{R_s}, e_1\rangle - \frac{1}{\sqrt{2}}|1_{L_s}, e_2\rangle$ in the hybrid system of nonlinear cavity plus the atom. **(a)** Atomic transition scheme: right- and left-handed circularly polarized idler photons (green spheres) off-resonantly ($\Delta_2 = \omega_e - \omega_i$) couple the ground state $|g\rangle$ to excited states $|e_1\rangle$ and $|e_2\rangle$, respectively. **(b)** The plot shows temporal evolution of the atom-photon entangled state $|\psi_{e_1,e_2}\rangle$, vacuum state $|0; g\rangle \equiv |0\rangle\,|g\rangle$ and single photon-pair entangled state $|\phi_1; g\rangle \equiv |\phi_1\rangle\,|g\rangle$. The nonlinear coupling strength is set to $A_p = 0.2\Omega$ (same as Fig. 2, CW pumping), and detunings are $\Delta_1 = \Delta_2 = 6\Omega$.

The detuning $\Delta_1 = \omega_p - \omega_s - \omega_i$, associated with the PDC process, and the detuning $\Delta_2 = \omega_e - \omega_i$, governing the atom–idler modes interaction, can be controlled by tuning the pump frequency ω_p and the cavity mode frequencies ω_s and ω_i. By appropriately choosing these frequencies, the condition $\Delta_1 = \Delta_2$ can be engineered. This corresponds to an effective energy-matching condition between the pump field and the joint excitation of the signal mode and the atom, $\omega_p = \omega_s + \omega_e$. Under this condition, the atom-cavity system can be driven from $|0; g\rangle$ into the entangled state $|\psi_{e_1,e_2}\rangle$. The underlying process can be understood as a series of higher-order transitions mediated by intermediate states. The dominant contribution arises from an effective second-order transition in which the initial state $|0; g\rangle$ couples to $|\psi_{e_1,e_2}\rangle$ via the off-resonant weakly populated intermediate state $|\phi_1; g\rangle$. Under the condition $\Delta_1 = \Delta_2$, the associated transition amplitude varies slowly in time, enabling constructive

interference and leading to an efficient buildup of population in $|\psi_{e_1,e_2}\rangle$, as shown in Fig. 3b.

Consistent with this understanding, in Fig. 3b, the $|\phi_1; g\rangle$ state is weakly excited and exhibits fast oscillations with period $\sim \frac{2\pi}{\Delta_1}$ due to the off-resonant PDC interaction. Furthermore, its direct coupling to $|0; g\rangle$ and $|\psi_{e_1,e_2}\rangle$ induces rapid oscillations in their populations, with the same characteristic timescale $\sim \frac{2\pi}{\Delta_1}$. We also see in Fig. 3b that $|\psi_{e_1,e_2}\rangle$ builds up on a slower time-scale, but eventually reaches a peak value and decreases again, following an oscillatory behavior, but with a much larger period than the fast oscillations of $|\phi_1; g\rangle$. Below, we analyze this effect further and present a way to take the probability of the $|\psi_{e_1,e_2}\rangle$ atom-photon entangled state beyond this peak value and close to the generation probability of 1.

Motivated by the separation of time scales between the main variations in the off-resonant ($|\phi_1; g\rangle$) and resonant states ($|0; g\rangle$ and $|\psi_{e_1,e_2}\rangle$), we derive an effective two-level description to analytically capture the slow oscillatory dynamics between the vacuum state $|0; g\rangle$ and the state $|\psi_{e_1,e_2}\rangle$. This is achieved by adiabatically eliminating the weak and fast dynamics associated with the intermediate state $|\phi_1; g\rangle$, yielding coupled differential equations that govern the coherent exchange of population between $|0; g\rangle$ and $|\psi_{e_1,e_2}\rangle$ (see Supplementary Material Sec. S2 for details of the derivation).

$$\begin{aligned} i\dot{C}_{0,\mathrm{g}}(t) &\approx \tfrac{2A_p^2}{\Delta_1}\, C_{0,\mathrm{g}}(t) + \tfrac{\sqrt{2}\Omega A_p}{\Delta_1}\, C_{e_1,e_2}(t), \\ i\dot{C}_{e_1,e_2}(t) &\approx \left(\tfrac{\Omega^2}{\Delta_1} + \tfrac{3A_p^2}{\Delta_1}\right) C_{e_1,e_2}(t) + \tfrac{\sqrt{2}\Omega A_p}{\Delta_1}\, C_{0,\mathrm{g}}(t). \end{aligned} \tag{1}$$

Here, $C_{0,\mathrm{g}}(t)$ denotes the probability amplitude associated with the vacuum state $|0; g\rangle$, while $C_{e_1,e_2}(t)$ corresponds to the probability amplitude of the atom–photon entangled state $|\psi_{e_1,e_2}\rangle$. The diagonal terms in these coupled differential equations (coefficients of $C_{0,\mathrm{g}}(t)$ in the first equation and $C_{e_1,e_2}(t)$ in the second equation) represent effective energy or Stark shifts of the two effective levels, while the off-diagonal terms define the effective coupling Rabi frequency $\Omega_{\mathrm{eff}} = \frac{\sqrt{2}A_p\Omega}{\Delta_1}$ between them. The Stark-shift difference is $\delta = \frac{\Omega^2}{\Delta_1}\left(1 + \left(\frac{A_p}{\Omega}\right)^2\right)$, which remains strictly non-zero, preventing exact resonance between the two effective levels. As a result, a complete population transfer from the $|0; g\rangle$ to $|\psi_{e_1,e_2}\rangle$ is not possible under these conditions, and an oscillatory back and forth population transfer with an effective period of $\frac{\pi}{\sqrt{\Omega_{\mathrm{eff}}^2 + (\delta/2)^2}}$ takes place, matching the observation in Fig. 3b. A detailed derivation of the solution of these coupled differential equations can be found in the Supplementary Material Sec. S2.

To fully understand the performance of the hybrid system in generation of the atom-photon entangled state $|\psi_{e_1,e_2}\rangle$ under the CW pumping condition, we show the maximum probability of generating $|\psi_{e_1,e_2}\rangle$ as a function of A_p and Δ_1 in Fig. 4b, together with the corresponding time at which this maximum is attained in Fig. 4a, which are obtained from the full numerical solution of the system without invoking adiabatic elimination.

From Fig. 4a, the time to reach maximum probability increases with Δ_1, consistent with Ω_{eff}, $\delta \propto 1/\Delta_1$, which slows the dynamics. As analytically predicted, the increase

in A_p reduces this time. In Fig. 4b, for small values of detuning Δ_1 and larger values of A_p, we see irregular behavior in the maximum probability, as the system lies in a non-adiabatic regime. As we move to larger detunings compared to A_p, the system gradually enters the adiabatic regime, resulting in a smooth and more regular behavior of the maximum probability. In Fig. 4c, we plot the maximum probability of generating the state $|\psi_{e_1,e_2}\rangle$ as a function of Δ_1/Ω for a fixed value of A_p/Ω. As the detuning Δ_1 increases, the maximum probability rises and gradually saturates once Δ_1 becomes sufficiently larger than A_p, corresponding to the onset of the adiabatic regime. In this regime, the analytical theory predicts that the maximum achievable probability becomes effectively independent of Δ_1 and depends only on the ratio A_p/Ω. In Fig. 4d, we compare the maximum probability obtained from numerical simulations for $\Delta_1 = 19\Omega$ with the analytical result derived from Eq. 1 (see Supplementary Material Sec. S2 for the analytical expression). The chosen detuning places the system in the adiabatic regime across the entire range of A_p considered. Specifically, the maximum probability initially increases with A_p, reaches a maximum near $A_p = \Omega$, and decreases for larger values $A_p > \Omega$. This non-monotonic dependence on $\frac{A_p}{\Omega}$ originates from the interplay between the effective coupling Ω_{eff} and the Stark-shift-induced detuning δ arising from Eq. 1. The δ is present for all values of A_p; however, its relative strength compared to the Ω_{eff} determines the efficiency of population transfer. While the Ω_{eff} scales linearly with $\frac{A_p}{\Omega}$, the Stark-shift difference δ scales as $\left(\frac{A_p}{\Omega}\right)^2$ and therefore grows more rapidly at larger A_p. As a result, for $A_p < \Omega$, the coupling (Ω_{eff}) dominates over the detuning (δ), leading to an increase in the maximum probability. In contrast, for $A_p > \Omega$, the δ becomes dominant, rendering the system effectively more off-resonant and thereby reducing the maximum probability. Consequently, a continuous-wave (CW) pump (with a constant phase and amplitude) cannot achieve deterministic excitation of the state $|\psi_{e_1,e_2}\rangle$ in our hybrid system. Nevertheless, the maximum probability achievable in this case is still two times larger than when generating the entangled state $|\phi_1\rangle$ via PDC in the absence of the atom, reaching a value of about 0.66.

Interestingly, this maximum probability limit for the generation of the state $|\psi_{e_1,e_2}\rangle$ can be overcome by applying a controlled phase modulation to the pump field, as illustrated in Fig. 5. In this case, still keeping the pump amplitude constant all along, we kept the pump phase constant during the initial stage of the evolution, allowing the population of the target state to grow up to its first maximum. At that instant, the pump phase is rapidly changed by π, corresponding to the transformation $A_p \to -A_p$ (see Supplementary Material Sec. S3 for details of how the phase change was modeled). Since the Stark shifts depend on $|A_p|^2$, they remain unchanged, whereas the sign of the effective coupling is reversed. As a result, the interference between previously accumulated and newly generated transition amplitudes is modified, enabling constructive buildup of the target-state population beyond its initial maximum. In Fig. 5, the dashed lines indicate the instants at which the pump phase is changed by π. In our simulations, for the chosen parameters ($A_1 = 0.2\Omega$ and $\Delta_1 = \Delta_2 = 6\Omega$), we implement two phase changes first from 0 to π, and subsequently from π back to 0. These phase changes enable near-complete transfer of population from the vacuum state to the atom–photon entangled state, with a maximum generation probability of

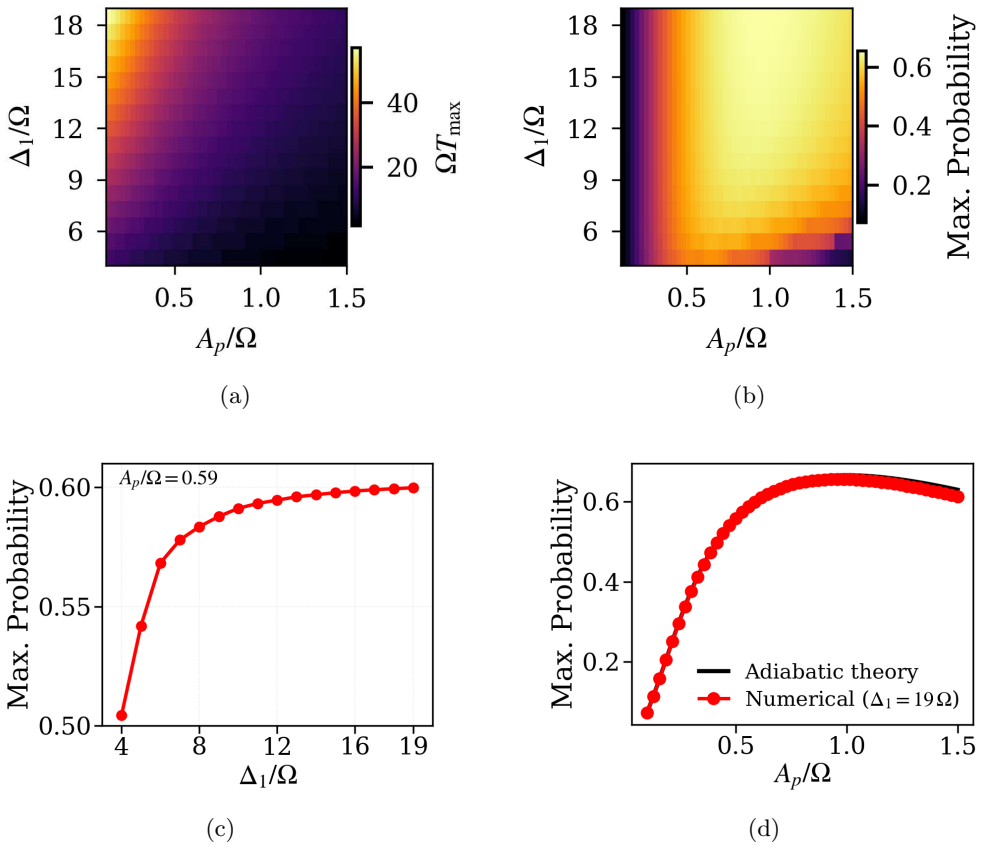


Fig. 4: Investigation of the maximum generation probability for the $|\psi_{e_1,e_2}\rangle$ atom-photon entangled state. **(a)** Time $T_{\max}$ required to reach the maximum population of the state $|\psi_{e_1,e_2}\rangle$ as a function of A_p/Ω and Δ_1/Ω. **(b)** Corresponding maximum probability of $|\psi_{e_1,e_2}\rangle$ over the same parameter space. **(c)** Maximum probability of $|\psi_{e_1,e_2}\rangle$ as a function of Δ_1/Ω for a fixed nonlinear coupling strength $A_p = 0.59\Omega$. **(d)** Maximum probability of $|\psi_{e_1,e_2}\rangle$ as a function of A_p/Ω for a fixed detuning $\Delta_1 = 19\Omega$, comparing the adiabatic theory (solid line) with numerical results (markers). (a-d) are all under the CW pumping condition.

0.985 for the state $|\psi_{e_1,e_2}\rangle$. In the Supplementary Material Sec. S3, we present a two-dimensional parameter scan over A_p and Δ_1. We observe that, for certain parameter regimes, a single phase change is sufficient to reach the near-deterministic regime for generation of the atom-photon entangled state, whereas for other regimes, multiple phase changes are required to achieve near-unit population transfer.

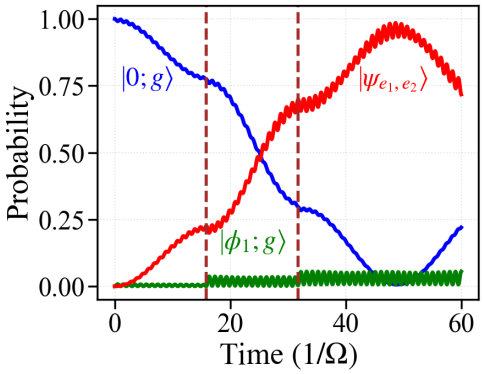


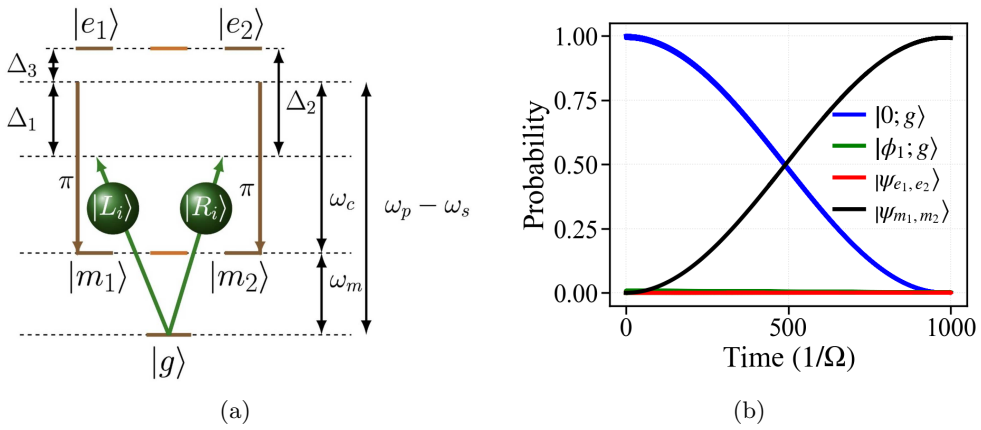
Fig. 5: Replacing the CW Pump field with a pump that has a constant amplitude but has a temporally varying phase profile. Here, the dashed lines indicate times at which the pump field experiences a smooth phase change from 0 to π and back. The overall dynamic results in the generation of the atom-photon entangled state $|\psi_{e_1,e_2}\rangle$ with the probability 0.985.

2.3 Deterministic generation of the atom-photon entanglement with the long-lived atomic states

In practice, excited states of atomic systems, similar to the one considered here, are prone to spontaneous decay, limiting the preservation of quantum information over long timescales, an essential requirement for establishing entanglement between distant quantum nodes. To enable long-lived storage of quantum information, we now extend the system by introducing long-lived atomic states $\{|m_1\rangle, |m_2\rangle\}$ with long coherence times (see Fig 1c). The Hamiltonian of the complete system is $\hat{H}_{NL}(t) + \hat{H}_{e\leftrightarrow g}(t) + \hat{H}_{e\leftrightarrow m}(t)$, where

$$\hat{H}_{e\leftrightarrow m}(t) = \hbar A_c \mathcal{E}_c(t) \left[|e_1\rangle \langle m_1| + |e_2\rangle \langle m_2|\right] e^{i\Delta_3 t} + H.c.$$

Here, A_c quantifies the coupling strength between the atom and the control field and is given by $A_c = \vec{d}_{e_{1,2}\leftrightarrow m_{1,2}} \cdot \vec{E}_c(\vec{r})/\hbar$. $\vec{E}_c(\vec{r})$ denotes the spatial mode profile and amplitude of the control field at the atomic position. We assume that the dipole transition matrix elements for the two transitions $|e\rangle_{1,2} \rightarrow |m\rangle_{1,2}$ have equal projections onto the polarization vector of the control field, given equal coupling strength for both transitions. A realistic implementation of this assumption using the level structure of ^{87}Rb is discussed in Sec. S5 of the Supplementary Material. $\mathcal{E}_c(t)$ is the slowly varying temporal envelope of the control pulse. In this section, we will continue with CW driving, i.e., $\mathcal{E}_c(t) = 1$. To facilitate $|e\rangle_i \rightarrow |m\rangle_i$ transitions, the control field is chosen to be π-polarized, enabling excitation transfer to the long-lived states with the same magnetic numbers as those of the corresponding excited states, as depicted in Fig 6a. The detuning $\Delta_3 = \omega_e - \omega_m - \omega_c$ characterizes the mismatch between the control field and the atomic transition $|m_i\rangle \leftrightarrow |e_i\rangle$. Here, we engineer the condition $\Delta_1 + \Delta_3 = \Delta_2$, which corresponds to an energy-matching relation $\omega_p = \omega_s + \omega_m + \omega_c$ (see Fig 6a).



(a) (b)

Fig. 6: Investigating the generation of the atom-photon entangled state $|\psi_{m_1,m_2}\rangle = \frac{1}{\sqrt{2}}|1_{R_s}, m_1\rangle - \frac{1}{\sqrt{2}}|1_{L_s}, m_2\rangle$ in the hybrid system of nonlinear cavity plus the atom. **(a)** Schematic of the atomic level transitions for a quantum memory. **(b)** Temporal evolution of state probabilities under continuous-wave (CW) driving of the pump and control fields simultaneously. The nonlinear coupling strength is $A_p = 0.2\Omega$, the atom–control-field coupling $A_c = 0.21\Omega$, and the detunings are $\Delta_1 = \Delta_3 = 6\Omega$ and $\Delta_2 = 12\Omega$.

This ensures that the pump field is resonant with the joint excitation of the signal mode, the atomic long-lived state, and the control field, thereby enabling an effective coupling between the vacuum state $|0;g\rangle$ and the state $|\psi_{m_1,m_2}\rangle$. The underlying process can be understood as a series of higher-order transitions mediated by intermediate states. The dominant contribution arises from an effective third-order transition in which $|0;g\rangle$ couples to $|\psi_{m_1,m_2}\rangle$ via the intermediate states $|\phi_1;g\rangle$ and $|\psi_{e_1,e_2}\rangle$, with the control field inducing the transfer to $|\psi_{m_1,m_2}\rangle$. Under the condition $\Delta_1 + \Delta_3 = \Delta_2$, the transition amplitude varies slowly in time, enabling constructive interference and leading to an efficient buildup of population in $|\psi_{m_1,m_2}\rangle$, as can be seen in Fig. 6b. In Fig. 6b, we can also see that the populations of the intermediate states $|\phi_1;g\rangle$ and $|\psi_{e_1,e_2}\rangle$ remain very small, as they only mediate the effective coupling between $|0;g\rangle$ and $|\psi_{m_1,m_2}\rangle$. Contrary to the case shown in Fig 3b, here, the population is transferred almost entirely from the vacuum state $|0;g\rangle$ to $|\psi_{m_1,m_2}\rangle$, using only CW pump and control fields (without the need for having phase changes), indicating near-deterministic generation of the target state for the chosen parameters.

To gain a more analytical understanding, we once again perform an adiabatic elimination of the intermediate states, which include $|\phi_1;g\rangle$ and $|\psi_{e_1,e_2}\rangle$(see Supplementary Material Sec. S4 for the details of the derivation). This approximation once again reduces the description of the overall system to a pair of differential equations describing the effective coupling between the vacuum and the long-lived atom-photon

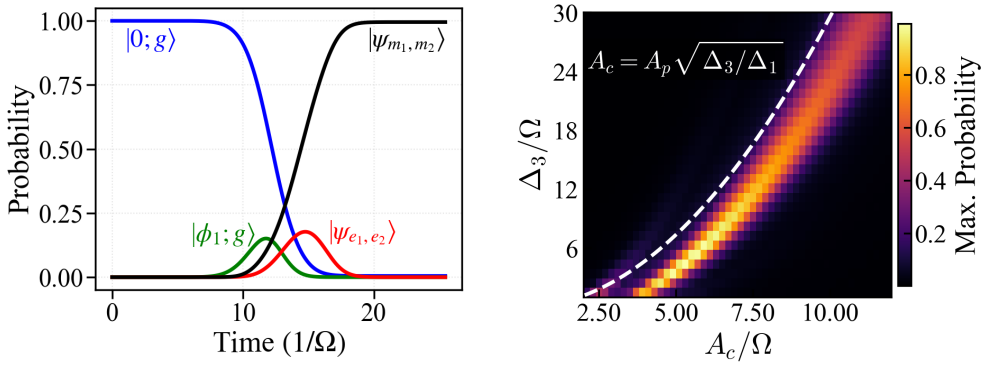
entangled state $|\psi_{m_1,m_2}\rangle$.

$$\begin{aligned} i\,\dot{C}_{0,g}(t) &= \tfrac{2A_p^2}{\Delta_1}\,C_{0,g}(t) - \tfrac{\sqrt{2}\,A_pA_c\Omega}{\Delta_1\Delta_3}\,C_{m_1,m_2}(t), \\ i\,\dot{C}_{m_1,m_2}(t) &= \left(\tfrac{3A_p^2}{\Delta_1} - \tfrac{A_c^2}{\Delta_3}\right)C_{m_1,m_2}(t) - \tfrac{\sqrt{2}\,A_pA_c\Omega}{\Delta_1\Delta_3}\,C_{0,g}(t). \end{aligned} \tag{2}$$

$C_{m_1,m_2}(t)$ is the probability amplitude associated with the atom-photon entangled state $|\psi_{m_1,m_2}\rangle$. Here, $\Omega^m_{\text{eff}} = \frac{\sqrt{2}\,A_pA_c\Omega}{\Delta_1\Delta_3}$ and $\delta_m = \frac{A_p^2}{\Delta_1} - \frac{A_c^2}{\Delta_3}$ denote the effective coupling and Stark-shift difference, respectively. A key difference from the previous case is that, in the presence of a control field, the Stark shift difference can be tuned to zero. This occurs when $A_c = A_p\sqrt{\frac{\Delta_3}{\Delta_1}}$, provided that the values of $\Delta_1, \Delta_3, A_p, A_c$ ensure the system operates in the regime where adiabatic elimination is valid. Under this condition, the effective detuning vanishes, rendering the system resonant and enabling complete population transfer from $|0;g\rangle$ to $|\psi_{m_1,m_2}\rangle$. Moreover, when the two effective levels are on resonance, the time T required for complete population transfer from $|0;g\rangle$ to the state $|\psi_{m_1,m_2}\rangle$ is determined solely by the effective coupling strength Ω^m_{eff}, given by $T = \frac{\pi}{2\Omega^m_{\text{eff}}}$. Thus, in the presence of a control field with optimized amplitude and detuning Δ_3, the generation of the entangled state $|\psi_{m_1,m_2}\rangle$ becomes fully deterministic, without requiring any temporal phase modulation of the pump or control fields. Furthermore, we can see that for δ_m to be zero, Δ_1 and Δ_3 must have the same signs.

2.4 Pulsed Excitation

So far, both the pump and control fields have been treated in the continuous-wave (CW) regime to clarify the underlying physics. However, in many quantum applications, pulsed excitation is used in practice, as it offers a natural way of controlling the duration and timing of the involved interactions. Furthermore, as will be shown here, operating the hybrid scheme under pulsed driving offers several advantages over the CW scheme. Although we have seen that CW pump and control fields can generate the light-matter entangled state deterministically, the required interaction time is very long in the case of generating $|\psi_{m_1,m_2}\rangle$ (see Fig 6b), making it challenging to preserve coherence over the full duration in practice. In principle, this time could be reduced by increasing the nonlinear coupling strength A_p (as can also be seen in Fig. 4a for generating $|\psi_{e_1,e_2}\rangle$), but doing so degrades the fidelity of the target state $|\psi_{m_1,m_2}\rangle$. Increasing the value of A_p pushes the system away from the adiabatic regime, resulting in an appreciable population of the off-resonant states $|\phi_1;g\rangle$ and $|\psi_{e_1,e_2}\rangle$, which in turn seed the population of higher-order states containing additional photons. The appearance of these unwanted states inevitably reduces the fidelity of the target atom–photon entangled state $|\psi_{m_1,m_2}\rangle$ (see Sec. S6 of the Supplementary Material for an example corresponding to larger values of A_p). Thus, in the CW driving regime, fully deterministic generation of the state $|\psi_{m_1,m_2}\rangle$ is achievable only when the system operates in a regime where the intermediate off-resonant states remains negligibly populated, such that the dynamics are governed by an effective direct coupling between $|0;g\rangle$ and $|\psi_{m_1,m_2}\rangle$, i.e., the system is in adiabatic regime.



(a) (b)

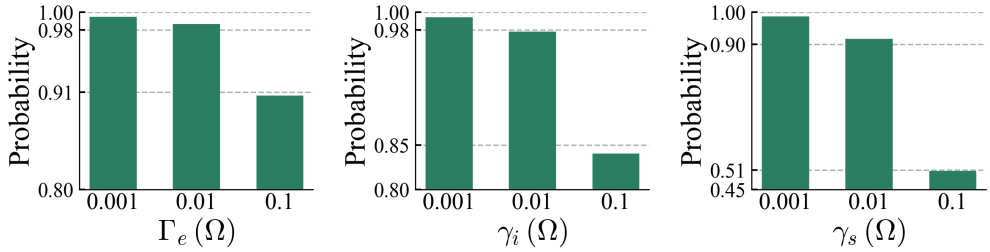
Fig. 7: Investigation of pulsed excitation for generating the $|\psi_{m_1,m_2}\rangle$ atom-photon entangled state. **(a)** Temporal evolution of state probabilities under pulsed excitation of the pump and control fields. The nonlinear coupling strength is $A_p = 10.07\Omega$, the atom–control-field coupling is $A_c = 5.5445\Omega$, and the detunings are $\Delta_1 = 30\Omega$, $\Delta_3 = 5\Omega$, and $\Delta_2 = 35\Omega$. **(b)** Maximum probability of generating the state $|\psi_{m_1,m_2}\rangle$ as a function of both Δ_3 and A_c. The white curve indicates the analytically predicted optimal values of A_c as a function of A_p, Δ_1, and Δ_3, for which complete population transfer from $|0;g\rangle$ to $|\psi_{m_1,m_2}\rangle$ is achieved in the adiabatic regime under continuous-wave (CW) pumping.

Interestingly, the use of pulsed drives offers a significant temporal advantage without compromising the fidelity in generating the target state $|\psi_{m_1,m_2}\rangle$. Crucially, pulsed driving enables a dynamical regime in which the population of the off-resonant intermediate states are further reduced compared to the CW regime. In the pulsed regime, the off-resonant excited states $|\phi_n;g\rangle$ and $|\psi_{e_1,e_2}\rangle$ are only transiently populated, as their amplitudes follow the pulse envelope and vanish once the driving field envelope decays to zero, since no resonant coupling exists to sustain their population (see Supplementary Material Sec. S7 for Pulsed PDC under off-resonant pumping). Thus, after the pulse, only the vacuum state $|0;g\rangle$ and the long-lived state $|\psi_{m_1,m_2}\rangle$ retain non-zero occupation probabilities. This permits the use of larger values of A_p and shorter pump and control pulses without populating higher-order photonic states $|\phi_n\rangle$, as these states are only transiently occupied and vanish after the pulse. In Fig. 7a, we show the state-generation probabilities for Gaussian pump and control pulses of identical temporal width, chosen as $\tau_p = \tau_c = 2.545/\Omega$. The corresponding spectral width of the pulse is approximately $\Delta\omega \sim 1/\tau_p$. We choose the value of A_p to be 50 times larger than that used in the adiabatic regime (Fig. 6b), while keeping Δ_1 sufficiently large compared to the pulse spectral width, i.e., $\Delta_1 \gg \Delta\omega \sim \frac{1}{\tau_p}$, such that the states $|\phi_n;g\rangle$ remain off-resonant without operating in the adiabatic regime. For optimal values of Δ_3 (namely $\Delta_1 + \Delta_3 = \Delta_2$), A_c, and pulse length, the timescale for complete population transfer to $|\psi_{m_1,m_2}\rangle$ is reduced by a factor of 50. Thus, enabling

near-deterministic generation of the state $|\psi_{m_1,m_2}\rangle$ with a probability of 0.995 on a significantly shorter timescale.

The optimal choices of A_c and the pulse duration can be guided by the analytical results obtained for the adiabatic regimes under CW driving (see the discussion after Eq. 2). However, the exact optimal values must be determined numerically, since the present protocol employs pulsed excitation and operates outside the regime where adiabatic elimination is valid. We illustrate this in Fig. 7b, which shows the dependence of the maximum probability of generating the state $|\psi_{m_1,m_2}\rangle$ on A_c and Δ_3 for pulsed excitation. An optimal region emerges in the (A_c, Δ_3) parameter space, where the population of $|\psi_{m_1,m_2}\rangle$ approaches unity. This narrow region can be understood from the approximate equalization of the Stark shifts, which minimizes the effective detuning between the states $|0; g\rangle$ and $|\psi_{m_1,m_2}\rangle$. Although this condition is derived within the adiabatic approximation, it remains a useful guideline in the quasi-adiabatic regime. The dashed curve corresponds to the analytical prediction for A_c obtained in the previous subsection and closely follows the numerically identified optimal region despite the system operating outside the strictly adiabatic regime. Furthermore, the maximum probability decreases with increasing Δ_3, consistent with the reduction of the effective coupling strength Ω^m_{eff}, which suppresses population transfer for a fixed pulse duration.

2.5 Impact of loss



(a) (b) (c)

Fig. 8: Maximum generation probability of the light–matter entangled state $|\psi_{m_1,m_2}\rangle$ as a function of different loss mechanisms. To investigate the effect of dissipation, we consider the pulsed driving scheme shown in Fig. 7a and use the same system parameters throughout. **(a)** Considering only the effect of the atomic spontaneous decay into the modes outside the cavity, with the rate Γ_e. Here, $\gamma_i = \gamma_s = 0$ i.e., the cavity is ideal. **(b)** Considering only the effect of the idler-mode cavity decay, with the rate γ_i. Here, $\gamma_s = \Gamma_e = 0$, i.e., the signal cavity mode is lossless and the atomic spontaneous emission outside the cavity is zero. **(c)** Considering only the effect of the signal-mode cavity decay, with the rate γ_s. Here, $\gamma_i = \Gamma_e = 0$.

Thus far, we have analyzed the system under idealized conditions, neglecting spontaneous emission into modes outside the cavity as well as cavity losses. In practice,

however, such dissipative processes are unavoidable. In this section, we investigate how different values of spontaneous decay rates of the atom outside the cavity mode, as well as cavity decay rates of the signal and idler modes, affect the maximum probability of generating the state $|\psi_{m_1,m_2}\rangle$. We have employed the Quantum Trajectories methodology [57] to study the impact of losses on our system, and we have described this methodology in the Method Section. We begin by analyzing the influence of spontaneous emission on the maximum probability of generating the state $|\psi_{m_1,m_2}\rangle$, under the assumption of an ideal, lossless cavity. The system under investigation is our pulsed case scenario, and we choose the system parameters to match those used in Fig. 7a, corresponding to the ideal lossless case.

In the simulation, we choose the spontaneous decay rates of the excited states of the atom outside the cavity modes as $\Gamma_e = \{0.001\Omega, 0.01\Omega, 0.1\Omega\}$. The associated jump operators employed in the quantum-trajectory formalism are $\sqrt{\Gamma_e}\,|g\rangle\langle e_1|$ and $\sqrt{\Gamma_e}\,|g\rangle\langle e_2|$, corresponding to spontaneous emission from $|e_1\rangle$ and $|e_2\rangle$ to the ground state $|g\rangle$. From Fig. 8a, we find that for atomic spontaneous emission rates of $\Gamma_e = 0.001\Omega$ and $\Gamma_e = 0.01\Omega$, the maximum generation probability of the state $|\psi_{m_1,m_2}\rangle$ remains close to the ideal case of 0.995. Specifically, the maximum probabilities are 0.994 for $\Gamma_e = 0.001\Omega$ and 0.985 for $\Gamma_e = 0.01\Omega$, indicating that the generation process remains near-deterministic. A significant drop occurs only when the spontaneous emission rate is increased to $\Gamma_e = 0.1\Omega$, for which the maximum probability drops to 0.91. As shown in Fig. 7a (see the red curve), the atomic excited state is populated only transiently over a time interval that is shorter than the total interaction time. The lifetime of the excited atomic state is given by $1/\Gamma_e$. For $\Gamma_e = 0.001\Omega$ and $\Gamma_e = 0.01\Omega$, this lifetime is much longer than the transient time window during which the atom has a non-negligible excitation probability. Consequently, the probability for a spontaneous emission event to occur during the evolution remains very small. But for $\Gamma_e = 0.1\Omega$, spontaneous emission becomes sufficiently strong to noticeably reduce the probability of generating the target atom–photon entangled state $|\psi_{m_1,m_2}\rangle$.

Next, we analyze the influence of idler-mode cavity losses on the maximum generation probability of $|\psi_{m_1,m_2}\rangle$, assuming a lossless signal mode ($\gamma_s = 0$) and zero atomic spontaneous decay outside the cavity ($\Gamma_e = 0$). We choose the idler decay rates as $\gamma_i = \{0.001\Omega, 0.01\Omega, 0.1\Omega\}$, with the associated jump operators given by $\sqrt{\gamma_i}\hat{a}_L$ and $\sqrt{\gamma_i}\hat{a}_R$, corresponding to photon loss from the left- and right-circularly polarized idler cavity modes, respectively. From Fig. 8b, we observe that the drop in the maximum probability is small and its close to the ideal value of 1 for $\gamma_i = 0.001\Omega$ and $\gamma_i = 0.01$. The observed behavior can be understood using the same reasoning as for spontaneous emission: the idler photons are populated only transiently over a time interval that is shorter than the total interaction time. For $\gamma_i \leq 0.01\Omega$, this transient population window is much shorter than the idler-mode lifetime $1/\gamma_i$, so the probability of idler-photon loss during the evolution remains negligible. A significant drop is obtained in the case when $\gamma_i = 0.1\Omega$, since then the idler cavity mode lifetime $\frac{1}{\gamma_i}$ is of the same order as the transient time window during which there is a non-negligible probability of finding idler photons in the cavity mode.

Finally, we investigate the influence of signal-mode cavity losses on the maximum generation probability of $|\psi_{m_1,m_2}\rangle$, while assuming a lossless idler mode and

vanishing atomic spontaneous decay. We choose the signal-mode decay rates as $\gamma_s = \{0.001\Omega, 0.01\Omega, 0.1\Omega\}$, with the corresponding jump operators given by $\sqrt{\gamma_s}\hat{b}_L$ and $\sqrt{\gamma_s}\hat{b}_R$, describing photon leakage from the left- and right-circularly polarized signal cavity modes, respectively. From Fig. 8c, we observe that the probability, as expected, is most sensitive to the signal-mode cavity decay rate γ_s. This occurs because the signal-mode excitation maintains a finite population throughout the interaction time, making the signal photon more susceptible to cavity losses.
As shown above, the individual loss channels are varied separately in order to isolate their effect on the generation probability of $|\psi_{m_1,m_2}\rangle$. To assess the experimental relevance of the parameter regimes investigated in this work, we compare them with experimentally reported cavity-QED parameters[47, 58–65] (see Table S1 in Sec. 8 of the Supplementary Material). Our simulations indicate that the protocol remains relatively robust against atomic spontaneous emission and idler-mode decay in the experimentally relevant regime, for example at $\Gamma_e/\Omega = 0.1$ and $\gamma_i/\Omega = 0.1$. In contrast, the signal-mode decay has a substantially stronger effect; for $\gamma_s/\Omega = 0.1$, the maximum generation probability is reduced to approximately 0.51. Since experimentally reported normalized cavity decay rates are typically of the order of 10^{-1} (see Table S1 in Sec. 8 of the Supplementary Material), signal-mode losses remain a significant challenge for the experimental realization of the proposed protocol. This motivates future loss-aware optimization strategies aimed at improving robustness against this loss channel [66].

3 Conclusion

We proposed and theoretically demonstrated that the hybridization of a nonlinear $\chi^{(2)}$ cavity with a multilevel atom enables deterministic generation of atom-photon entangled states of different kinds, an essential building block for scalable quantum networks. The deterministic nature of the process is particularly significant as it eliminates the need for probabilistic heralding or multiplexing strategies that typically limit the scalability and rate of conventional entanglement-distribution schemes. The frequency tunability of the system, governed by the conservation of energy conditions, allows flexible spectral matching across different quantum nodes, enabling a hybrid interconnectedness between disparate quantum systems.

Moreover, the hybrid systems offers much versatility in engineering the entangled-light matter state, as the spatial, spectral, and polarization properties of the nonlinear part of the system can be strongly tailored by carefully shaping the modal properties of the nonlinear cavity. Hence, we believe that this hybridization concept can be extended to other types of quantum memories and entanglement in other photonic degrees of freedom. The main strong requirement is that the quantum memory has to be of an atom-like property, where a level can only store one quanta of excitation.

Overall, this architecture offers a promising pathway toward high-fidelity, on-demand quantum network nodes capable of coherent entanglement distribution and storage across long distances.

Methods

Numerical framework

The system dynamics were investigated by numerically solving the time-dependent Schrödinger equation in the interaction picture using the Quantum Toolbox in Python (QuTiP). The total Hilbert space consisted of the cavity modes together with the multilevel atomic system, represented within a truncated Hilbert space. For coherent (unitary) evolution, the dynamics were propagated using the `sesolve` solver, while open quantum dynamics including dissipation were simulated using the Monte-Carlo wavefunction solver `mcsolve`.

Hilbert-Space truncation

To make the simulations numerically tractable, we adopted a truncated Hilbert space retaining the relevant photonic and atomic states. Specifically, the photonic Fock basis of both the signal and idler cavity modes was truncated. The simulations shown in Fig. 2a, 2b, 3b, 5, 6b and 7a were performed with the signal and idler modes truncated up to $n = 10$. The simulation in Fig. 4 is done with truncation $n = 30$ for signal and idler modes. The simulation in Fig. 7b is done with truncation up to $n = 15$ for signal and idler modes. The truncation parameter n was chosen larger than the value required to ensure convergence of the numerical results.

Pulse modeling

Time-dependent pump and control fields were implemented through explicit time-dependent coefficients in the interaction-picture Hamiltonian. Unless otherwise stated, Gaussian pump and control pulses of identical temporal width were assumed, with pulse duration $\tau_p = \tau_c = 2.545/\Omega$. The envelope was of the following form: $e^{-\frac{(t-t_0)^2}{2\tau_p^2}}$

Open Quantum System Dynamics using Quantum Trajectories

To solve the open quantum dynamics, we have employed the Quantum Monte Carlo Trajectory Method in QuTiP. The observable over here is the projector of the state $|\psi_{m_1,m_2}\rangle$ i.e., $\hat{O} = |\psi_{m_1,m_2}\rangle \langle\psi_{m_1,m_2}|$. For each trajectory, we calculate the expectation value of this observable at each instant of time. To calculate the probability, we take the mean of this expectation value over all the trajectories.

$$P_{m_1,m_2}(t) = \sum_{i=1}^{N} \frac{\langle\psi_i(t)|\hat{O}|\psi_i(t)\rangle}{N} = \sum_{i=1}^{N} \frac{P^i_{m_1,m_2}(t)}{N} \tag{3}$$

Where N is the number of trajectories and $|\psi_i(t)\rangle$ is the state of the system. The variance in the probability at an instant is:

$$(\Delta P_{m_1,m_2}(t))^2 = \frac{1}{N-1} \sum_{i=1}^{N} (P^i_{m_1,m_2}(t) - P_{m_1,m_2}(t))^2 \tag{4}$$

Finally, the standard error of mean $P^{SEM}_{m_1,m_2}(t)$ is:

$$P^{SEM}_{m_1,m_2}(t) = \frac{\Delta P_{m_1,m_2}(t)}{\sqrt{N}} \tag{5}$$

The number of Trajectories depends on the value of decay constants. For the largest decay constant value $\Gamma_e = \gamma_i = \gamma_s = 0.1\Omega$ we have employed 60000 Trajectories to keep the standard error of the mean of the order 10^{-3} as shown in Figure 9. For the other two decay constant values, we have used 40000 Trajectories, keeping the standard error of the mean of the order 10^{-4}.

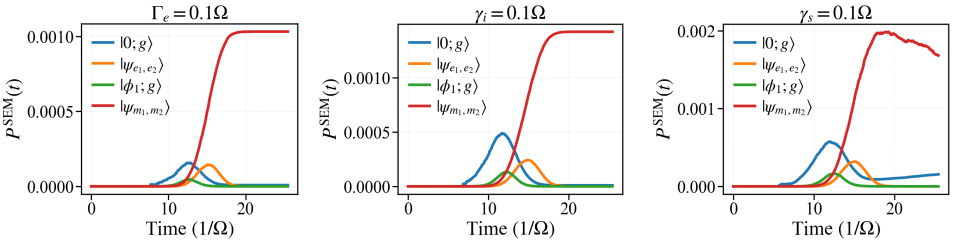


Fig. 9: Standard error of the mean (SEM) obtained from the Monte Carlo simulations in QuTiP for the populations of the states $|0;g\rangle$, $|\psi_{e_1,e_2}\rangle$, $|\phi_1;g\rangle$, and $|\psi_{m_1,m_2}\rangle$. The panels correspond to (left) atomic spontaneous emission $\Gamma_e = 0.1\Omega$, (middle) idler-mode loss $\gamma_i = 0.1\Omega$, and (right) signal-mode loss $\gamma_s = 0.1\Omega$. The time variable t is expressed in units of $1/\Omega$.

Data availability

The data supporting the findings of this study are available from the corresponding author upon reasonable request.

Code availability

The numerical code used to generate the results and figures is available from the corresponding author upon reasonable request.

Competing interests

The authors declare no competing interests.

Author contributions

P.T. performed the analytical and numerical calculations and wrote the first draft of the manuscript. A.K. contributed to technical discussions and to writing the first

draft. S.S. conceived and supervised the project. F.S. and R.L. contributed to scientific discussions. S.S. and F.S. secured funding. All authors discussed the results, reviewed the manuscript, and approved the final version.

Acknowledgements

This research was supported by the Carl Zeiss Foundation (CZS Center QPhoton), the German Research Foundation (DFG) under Project ID 398816777—SFB 1375 (NOA), and the German Federal Ministry of Education and Research (BMBF) under Project ID 13N16108 (PhoQuant). S.S. further acknowledges support from the Nexus program of the Carl Zeiss Foundation through the MetaNN project (Project ID P2022-04-018).

References

[1] Fang, K., Zhao, J., Li, X., Li, Y., Duan, R.: Quantum network: from theory to practice. Science China Information Sciences **66**(8) (2023) https://doi.org/10.1007/s11432-023-3773-4

[2] Azuma, K., Economou, S.E., Elkouss, D., Hilaire, P., Jiang, L., Lo, H.-K., Tzitrin, I.: Quantum repeaters: From quantum networks to the quantum internet. Reviews of Modern Physics **95**(4) (2023) https://doi.org/10.1103/revmodphys.95.045006

[3] Kimble, H.J.: The quantum internet. Nature **453**(7198), 1023–1030 (2008) https://doi.org/10.1038/nature07127

[4] Briegel, H.-J., Dür, W., Cirac, J.I., Zoller, P.: Quantum repeaters: The role of imperfect local operations in quantum communication. Phys. Rev. Lett. **81**, 5932–5935 (1998) https://doi.org/10.1103/PhysRevLett.81.5932

[5] Couteau, C.: Quantum computing using photons. The European Physical Journal A **61**(4), 75 (2025) https://doi.org/10.1140/epja/s10050-025-01517-5

[6] Canteri, M., Koong, Z.X., Bate, J., Winkler, A., Krutyanskiy, V., Lanyon, B.P.: Photon-interfaced ten-qubit register of trapped ions. Phys. Rev. Lett. **135**, 080801 (2025) https://doi.org/10.1103/v5k1-whwz

[7] Gangloff, D.: An optical interface for quantum networks. Science **378**(6619), 473–474 (2022) https://doi.org/10.1126/science.ade6964 https://www.science.org/doi/pdf/10.1126/science.ade6964

[8] Liu, X., Hu, J., Li, Z.-F., Li, X., Li, P.-Y., Liang, P.-J., Zhou, Z.-Q., Li, C.-F., Guo, G.-C.: Heralded entanglement distribution between two absorptive quantum memories. Nature **594**(7861), 41–45 (2021) https://doi.org/10.1038/s41586-021-03505-3

[9] Heshami, K., England, D.G., Humphreys, P.C., Bustard, P.J., Acosta, V.M., Nunn, J., Sussman, B.J.: Quantum memories: emerging applications and recent

advances. Journal of Modern Optics **63**(20), 2005–2028 (2016) https://doi.org/10.1080/09500340.2016.1148212

[10] Sabooni, M., Li, Q., Kröll, S., Rippe, L.: Efficient quantum memory using a weakly absorbing sample. Phys. Rev. Lett. **110**, 133604 (2013) https://doi.org/10.1103/PhysRevLett.110.133604

[11] Zukowski, M., Zeilinger, A., Horne, M.A., Ekert, A.K.: "event-ready-detectors" bell experiment via entanglement swapping. Phys. Rev. Lett. **71**, 4287–4290 (1993) https://doi.org/10.1103/PhysRevLett.71.4287

[12] Lago-Rivera, D., Grandi, S., Rakonjac, J.V., Seri, A., Riedmatten, H.: Telecom-heralded entanglement between multimode solid-state quantum memories. Nature **594**(7861), 37–40 (2021) https://doi.org/10.1038/s41586-021-03481-8

[13] Simon, C., Riedmatten, H., Afzelius, M., Sangouard, N., Zbinden, H., Gisin, N.: Quantum repeaters with photon pair sources and multimode memories. Phys. Rev. Lett. **98**, 190503 (2007) https://doi.org/10.1103/PhysRevLett.98.190503

[14] Sangouard, N., Simon, C., Riedmatten, H., Gisin, N.: Quantum repeaters based on atomic ensembles and linear optics. Rev. Mod. Phys. **83**, 33–80 (2011) https://doi.org/10.1103/RevModPhys.83.33

[15] Wolters, J., Buser, G., Horsley, A., Béguin, L., Jöckel, A., Jahn, J.-P., Warburton, R.J., Treutlein, P.: Simple atomic quantum memory suitable for semiconductor quantum dot single photons. Physical Review Letters **119**(6) (2017) https://doi.org/10.1103/physrevlett.119.060502

[16] Drmota, P., Main, D., Nadlinger, D.P., Nichol, B.C., Weber, M.A., Ainley, E.M., Agrawal, A., Srinivas, R., Araneda, G., Ballance, C.J., Lucas, D.M.: Robust quantum memory in a trapped-ion quantum network node. Phys. Rev. Lett. **130**, 090803 (2023) https://doi.org/10.1103/PhysRevLett.130.090803

[17] Cho, Y.-W., Kim, Y.-H.: Atomic vapor quantum memory for a photonic polarization qubit. Optics Express **18**(25), 25786–25793 (2010) https://doi.org/10.1364/OE.18.025786

[18] Buser, G., Mottola, R., Cotting, B., Wolters, J., Treutlein, P.: Single-photon storage in a ground-state vapor cell quantum memory. PRX Quantum **3**, 020349 (2022) https://doi.org/10.1103/PRXQuantum.3.020349

[19] Sayat, M.T., Lee, T.R., Negi, S., Iwahara, N., Seo, I.C., Tan, Y.C., Lam, P.K., Cho, Y.-W., Soh, J.-R.: Polarisation and temperature dependence of er3+:cawo4—towards a solid-state rare-earth ion-doped quantum memory. Physica Scripta **101**(6), 065104 (2026) https://doi.org/10.1088/1402-4896/ae3e21

[20] Gündoğan, M., Ledingham, P.M., Kutluer, K., Mazzera, M., Riedmatten, H.:

Solid state spin-wave quantum memory for time-bin qubits. Phys. Rev. Lett. **114**, 230501 (2015) https://doi.org/10.1103/PhysRevLett.114.230501

[21] Couteau, C.: Spontaneous parametric down-conversion. Contemporary Physics **59**(3), 291–304 (2018) https://doi.org/10.1080/00107514.2018.1488463 https://doi.org/10.1080/00107514.2018.1488463

[22] Slattery, O.T., Ma, L., Zong, K., Tang, X.: Background and review of cavity-enhanced spontaneous parametric down-conversion. Journal of Research of the National Institute of Standards and Technology **124**, 124019 (2019) https://doi.org/10.6028/jres.124.019

[23] Wang, H., Zeng, Q., Ma, H., Yuan, Z.: Progress on chip-based spontaneous four-wave mixing quantum light sources. Advanced Devices & Instrumentation **5**, 0032 (2024) https://doi.org/10.34133/adi.0032 https://spj.science.org/doi/pdf/10.34133/adi.0032

[24] Son, C., Peana, S., Matthiessen, O., Kryvobok, A., Senichev, A., Boltasseva, A., Shalaev, V.M., Chekhova, M.: Generation of photon pairs through spontaneous four-wave mixing in subwavelength nonlinear films. Opt. Lett. **50**(13), 4434–4437 (2025) https://doi.org/10.1364/OL.565864

[25] Wang, Y., Jöns, K.D., Sun, Z.: Integrated photon-pair sources with nonlinear optics. Applied Physics Reviews **8**(1), 011314 (2021) https://doi.org/10.1063/5.0030258

[26] Fekete, J., Rieländer, D., Cristiani, M., Riedmatten, H.: Ultranarrow-band photon-pair source compatible with solid state quantum memories and telecommunication networks. Phys. Rev. Lett. **110**, 220502 (2013) https://doi.org/10.1103/PhysRevLett.110.220502

[27] Shapiro, J.H., Raymer, M.G., Embleton, C., Wong, F.N.C., Smith, B.J.: Entanglement source and quantum memory analysis for zero-added-loss multiplexing. Phys. Rev. Appl. **22**, 044014 (2024) https://doi.org/10.1103/PhysRevApplied.22.044014

[28] Christ, A., Silberhorn, C.: Limits on the deterministic creation of pure single-photon states using parametric down-conversion. Physical Review A **85**, 023829 (2012) https://doi.org/10.1103/PhysRevA.85.023829

[29] Tsai, P.-J., Hsiao, Y.-F., Chen, Y.-C.: Quantum storage and manipulation of heralded single photons in atomic memories based on electromagnetically induced transparency. Phys. Rev. Res. **2**, 033155 (2020) https://doi.org/10.1103/PhysRevResearch.2.033155

[30] Tseng, Y.-C., Wei, Y.-C., Chen, Y.-C.: Efficient quantum memory for photonic

polarization qubits generated by cavity-enhanced spontaneous parametric down-conversion. Opt. Express **30**(11), 19944–19960 (2022) https://doi.org/10.1364/OE.460026

[31] Duan, L.-M., Monroe, C.: Colloquium: Quantum networks with trapped ions. Rev. Mod. Phys. **82**, 1209–1224 (2010) https://doi.org/10.1103/RevModPhys.82.1209

[32] Lounis, B., Orrit, M.: Single-photon sources. Reports on Progress in Physics **68**(5), 1129–1179 (2005) https://doi.org/10.1088/0034-4885/68/5/R04

[33] Reiserer, A., Rempe, G.: Cavity-based quantum networks with single atoms and optical photons. Rev. Mod. Phys. **87**, 1379–1418 (2015) https://doi.org/10.1103/RevModPhys.87.1379

[34] Cirac, J.I., Zoller, P., Kimble, H.J., Mabuchi, H.: Quantum state transfer and entanglement distribution among distant nodes in a quantum network. Phys. Rev. Lett. **78**, 3221–3224 (1997) https://doi.org/10.1103/PhysRevLett.78.3221

[35] Ritter, S., Nölleke, C., Hahn, C., Reiserer, A., Neuzner, A., Uphoff, M., Mücke, M., Figueroa, E., Bochmann, J., Rempe, G.: An elementary quantum network of single atoms in optical cavities. Nature **484**(7393), 195–200 (2012) https://doi.org/10.1038/nature11023

[36] Mücke, M., Bochmann, J., Hahn, C., Neuzner, A., Nölleke, C., Reiserer, A., Rempe, G., Ritter, S.: Generation of single photons from an atom-cavity system. Physical Review A **87**(6) (2013) https://doi.org/10.1103/physreva.87.063805

[37] Vitanov, N.V., Rangelov, A.A., Shore, B.W., Bergmann, K.: Stimulated raman adiabatic passage in physics, chemistry, and beyond. Rev. Mod. Phys. **89**, 015006 (2017) https://doi.org/10.1103/RevModPhys.89.015006

[38] Cohen, M., Martin, A., Dalidet, R., Pastier, F., Billard, M., Lemaitre, A., Giesz, V., Somaschi, N., Thomas, S., Senellart-Mardon, P., Tanzilli, S., Labonté, L.: Compact and efficient quantum frequency conversion of a fiber-pigtailed single-photon source. APL Quantum **3**(1), 016101 (2026) https://doi.org/10.1063/5.0292682

[39] Brevoord, J.M., Geus, J.F., Turan, T., Romero, M.G., Rodríguez, D.B., Codreanu, N., Stramma, A.M., Hanson, R., Elsen, F., Jungbluth, B.: Quantum frequency conversion of single photons from a tin-vacancy center in diamond. Optica Quantum **3**(6), 583–589 (2025) https://doi.org/10.1364/OPTICAQ.576448

[40] Saravi, S., Poddubny, A.N., Pertsch, T., Setzpfandt, F., Sukhorukov, A.A.: Atom-mediated spontaneous parametric down-conversion in periodic waveguides. Opt. Lett. **42**(22), 4724–4727 (2017) https://doi.org/10.1364/OL.42.004724

[41] Krstić, A., Tiwari, P., Höhe, F., Setzpfandt, F., Peschel, U., Ankerhold, J., Saravi, S.: Hybrid source of quantum light for generation of frequency tunable fock states. Phys. Rev. Lett. **133**, 203605 (2024) https://doi.org/10.1103/PhysRevLett.133.203605

[42] Akat'ev, D.O., Kalachev, A.A.: Optical parametric oscillator with quantum memory for quantum repeaters. Laser Physics **33**(1), 015202 (2023) https://doi.org/10.1088/1555-6611/aca6dc

[43] Qin, W., Miranowicz, A., Li, P.-B., Lü, X.-Y., You, J.Q., Nori, F.: Exponentially enhanced light-matter interaction, cooperativities, and steady-state entanglement using parametric amplification. Phys. Rev. Lett. **120**, 093601 (2018) https://doi.org/10.1103/PhysRevLett.120.093601

[44] Wang, X., Qin, W., Miranowicz, A., Savasta, S., Nori, F.: Unconventional cavity optomechanics: Nonlinear control of phonons in the acoustic quantum vacuum. Phys. Rev. A **100**, 063827 (2019) https://doi.org/10.1103/PhysRevA.100.063827

[45] Zhou, Y., Malik, P., Fertig, F., Bock, M., Bauer, T., Leent, T., Zhang, W., Becher, C., Weinfurter, H.: Long-lived quantum memory enabling atom-photon entanglement over 101 km of telecom fiber. PRX Quantum **5**, 020307 (2024) https://doi.org/10.1103/PRXQuantum.5.020307

[46] Jutisz, M., Erl, A., Wolters, J., Gundogan, M., Krutzik, M.: Stand-alone mobile quantum memory system. Phys. Rev. Appl. **23**, 024045 (2025) https://doi.org/10.1103/PhysRevApplied.23.024045

[47] Specht, H.P., Nölleke, C., Reiserer, A., Uphoff, M., Figueroa, E., Ritter, S., Rempe, G.: A single-atom quantum memory. Nature **473**, 190–193 (2011) https://doi.org/10.1038/nature09997

[48] Reiserer, A., Rempe, G.: Cavity-based quantum networks with single atoms and optical photons. arXiv preprint (2015) 1412.2889. arXiv:1412.2889v2 [quant-ph]

[49] Lindner, N.H., Rudolph, T.: Proposal for pulsed on-demand sources of photonic cluster state strings. Phys. Rev. Lett. **103**, 113602 (2009) https://doi.org/10.1103/PhysRevLett.103.113602

[50] Schwartz, I., Cogan, D., Schmidgall, E.R., Don, Y., Gantz, L., Kenneth, O., Lindner, N.H., Gershoni, D.: Deterministic generation of a cluster state of entangled photons. Science **354**(6311), 434–437 (2016) https://doi.org/10.1126/science.aah4758

[51] Mataji-Kojouri, A., Liscidini, M.: Narrow-band photon pair generation through cavity-enhanced spontaneous parametric down-conversion. Phys. Rev. A **108**, 053714 (2023) https://doi.org/10.1103/PhysRevA.108.053714

[52] Pan, J.-W., Chen, Z.-B., Lu, C.-Y., Weinfurter, H., Zeilinger, A., Zukowski, M.: Multiphoton entanglement and interferometry. Reviews of Modern Physics **84**(2), 777–838 (2012) https://doi.org/10.1103/RevModPhys.84.777

[53] Kok, P., Braunstein, S.L.: Postselected versus nonpostselected quantum teleportation using parametric down-conversion. Phys. Rev. A **61**, 042304 (2000) https://doi.org/10.1103/PhysRevA.61.042304

[54] Lamas-Linares, A., Howell, J.C., Bouwmeester, D.: Stimulated emission of polarization-entangled photons. Nature **412**(6849), 887–890 (2001) https://doi.org/10.1038/35091014

[55] Sakurai, J.J., Napolitano, J.: Modern Quantum Mechanics, 3rd edn. Cambridge University Press, Cambridge (2020)

[56] Wang, P., Hiltunen, E.O., Schotland, J.C.: Rotating wave approximation and renormalized perturbation theory. Journal of Physics A: Mathematical and Theoretical **59**(14), 145302 (2026) https://doi.org/10.1088/1751-8121/ae551f

[57] Daley, A.J.: Quantum trajectories and open many-body quantum systems. Advances in Physics **63**(2), 77–149 (2014) https://doi.org/10.1080/00018732.2014.933502

[58] Grinkemeyer, B., Guardado-Sanchez, E., Dimitrova, I., Shchepanovich, D., Mandopoulou, G.E., Borregaard, J., Vuletić, V., Lukin, M.D.: Error-detected quantum operations with neutral atoms mediated by an optical cavity. Science **387**(6740), 1301–1305 (2025) https://doi.org/10.1126/science.adr7075 https://www.science.org/doi/pdf/10.1126/science.adr7075

[59] Hood, C.J., Chapman, M.S., Lynn, T.W., Kimble, H.J.: Real-time cavity qed with single atoms. Phys. Rev. Lett. **80**, 4157–4160 (1998) https://doi.org/10.1103/PhysRevLett.80.4157

[60] Ye, J., Vernooy, D.W., Kimble, H.J.: Trapping of single atoms in cavity qed. Phys. Rev. Lett. **83**, 4987–4990 (1999) https://doi.org/10.1103/PhysRevLett.83.4987

[61] Maunz, P., Puppe, T., Schuster, I., Syassen, N., Pinkse, P.W.H., Rempe, G.: Cavity cooling of a single atom. Nature **428**(6978), 50–52 (2004) https://doi.org/10.1038/nature02387

[62] Deist, E., Lu, Y.-H., Ho, J., Pasha, M.K., Zeiher, J., Yan, Z., Stamper-Kurn, D.M.: Mid-circuit cavity measurement in a neutral atom array. Phys. Rev. Lett. **129**, 203602 (2022) https://doi.org/10.1103/PhysRevLett.129.203602

[63] Wang, Z., Guan, S., Teng, G., Yang, P., Zhang, P., Li, G., Zhang, T.: A cavity qed system with defect-free single-atom array strongly coupled to an optical cavity. Quantum Frontiers **4**, 10 (2025) https://doi.org/10.1007/s44214-025-00083-7

[64] Liu, Y., Wang, Z., Yang, P., Wang, Q., Fan, Q., Guan, S., Li, G., Zhang, P., Zhang, T.: Realization of strong coupling between deterministic single-atom arrays and a high-finesse miniature optical cavity. Phys. Rev. Lett. **130**, 173601 (2023) https://doi.org/10.1103/PhysRevLett.130.173601

[65] Thomas, P., Ruscio, L., Morin, O., Rempe, G.: Efficient generation of entangled multiphoton graph states from a single atom. Nature **608**(7924), 677–681 (2022) https://doi.org/10.1038/s41586-022-04987-5

[66] Stodd, B., Tiwari, P., Sondenheimer, R., Saravi, S., Gärttner, M.: Loss-aware pulse sequence optimization for generating photonic Fock states (2026). https://arxiv.org/abs/2606.27158

Supplementary Files

This is a list of supplementary files associated with this preprint. Click to download.

- Supplemenatry.pdf